Interfacial Electron-Phonon Coupling Constants Extracted from Intrinsic Replica Bands in Monolayer $FeSe/SrTiO_3$

Brendan D. Faeth,[1,*] Saien Xie,[1] Shuolong Yang,[1,2,3,‡] Jason K. Kawasaki,[1,2,§] Jocienne N. Nelson,[1] Shuyuan Zhang,[1] Christopher Parzyck,[1] Pramita Mishra,[1,‖] Chen Li,[1] Christopher Jozwiak,[4] Aaron Bostwick,[4] Eli Rotenberg,[4] Darrell G. Schlom,[3,2] and Kyle M. Shen[1,2,†]

[1]*Department of Physics, Laboratory of Atomic and Solid State Physics, Cornell University, Ithaca, New York 14853, USA*
[2]*Kavli Institute at Cornell for Nanoscale Science, Ithaca, New York 14853, USA*
[3]*Department of Materials Science and Engineering, Cornell University, Ithaca, New York 14853, USA*
[4]*Advanced Light Source, E.O. Lawrence Berkeley National Laboratory, Berkeley, California 94720, USA*

(Received 5 February 2021; revised 26 April 2021; accepted 19 May 2021; published 30 June 2021)

The observation of replica bands by angle-resolved photoemission spectroscopy has ignited interest in the study of electron-phonon coupling at low carrier densities, particularly in monolayer $FeSe/SrTiO_3$, where the appearance of replica bands has motivated theoretical work suggesting that the interfacial coupling of electrons in the FeSe layer to optical phonons in the $SrTiO_3$ substrate might contribute to the enhanced superconducting pairing temperature. Alternatively, it has also been recently proposed that such replica bands might instead originate from extrinsic final state losses associated with the photoemission process. Here, we perform a quantitative examination of replica bands in monolayer $FeSe/SrTiO_3$, where we are able to conclusively demonstrate that the replica bands are indeed signatures of intrinsic electron-boson coupling, and not associated with final state effects. A detailed analysis of the energy splittings and relative peak intensities between the higher-order replicas, as well as other self-energy effects, allows us to determine that the interfacial electron-phonon coupling in the system corresponds to a value of $\lambda = 0.19 \pm 0.02$, providing valuable insights into the enhancement of superconductivity in monolayer $FeSe/SrTiO_3$. The methodology employed here can also serve as a new and general approach for making more rigorous and quantitative comparisons to theoretical calculations of electron-phonon interactions and coupling constants.

DOI: 10.1103/PhysRevLett.127.016803

One of the most powerful attributes of angle-resolved photoemission spectroscopy (ARPES) is its ability to reveal many-body interactions through its line shape, owing to its close relationship to the single-particle spectral function $A(\mathbf{k}, \omega)$. ARPES has revealed the presence of strong electron-boson coupling in a variety of quantum materials, including high-temperature cuprate superconductors [1,2], colossal magnetoresistive manganites [3], and titanates [4]. At high carrier densities, electron-boson coupling is manifested as an abrupt kink in the quasiparticle dispersion occurring at the boson energy. At low carrier densities, where screening is weaker and the Fermi energy, E_F, can be comparable to the relevant phonon frequency, Ω_0, the electron-phonon coupling can give rise to polaronic quasiparticles and the presence of satellite "replica bands," which occur at near-integer multiples of Ω_0. Such features have been recently reported in a variety of systems, including at the surface of $SrTiO_3$ [4–6], anatase TiO_2 [7,8], and most notably in monolayer FeSe films grown on $SrTiO_3$ [9–12], where it has been argued that the interfacial coupling of electrons in the FeSe monolayer to optical phonons in the $SrTiO_3$ substrate could potentially be responsible for its enhanced superconducting properties [9]. On the other hand, it has also been recently suggested that these replica bands observed by ARPES are not signatures of intrinsic electron-phonon interactions, but rather could arise from extrinsic electron energy losses in the photoemission process, whereby ejected photoelectrons lose energy to surface phonons [13]. Such extrinsic "final-state effects" produced by photoelectron energy loss processes would appear very similar to intrinsic satellites. Further complicating the situation, such loss features should be prevalent in systems where the carrier density is low and screening effects are weak, precisely where polaronic quasiparticles and intrinsic replica bands in ARPES would also be expected.

Therefore, a detailed investigation of photoemission replica bands is imperative to distinguish whether they are indeed intrinsic features in the spectral function of quantum materials versus extrinsic final-state loss effects. Given the importance of ARPES as the premier tool for investigating electronic many-body interactions, this is critical not only for the understanding of ARPES as a technique, but also for the general study of quantum materials and many-body interactions. Furthermore, a more rigorous analysis of the experimental replica bands,

including their intensities and energy separations, can help to inform and constrain theoretical models which tackle the long-standing problem of electron-lattice interactions in quantum materials. To achieve this, we investigate molecular beam epitaxy (MBE)-grown, single layer $FeSe/SrTiO_3$ thin films, where such replica bands have been observed, but also where it has been suggested as potentially arising from extrinsic loss effects from Fuchs-Kliewer phonons in the $SrTiO_3$ substrate [14]. By employing a wide range of photon energies, we are able to conclusively determine that the replica bands indeed arise from intrinsic electron-phonon coupling between the FeSe film and $SrTiO_3$ substrate, and not from extrinsic losses. A quantitative analysis of the spectra in comparison to prior theoretical calculations also allows us to determine the coupling constant, $\lambda = 0.19 \pm 0.02$, by simultaneously extracting the blueshift of the first satellite feature as well as the relative intensities of the replica bands to the main band which place tight constraints on theoretical models. This work not only demonstrates that replica bands in $FeSe/SrTiO_3$ arise from intrinsic electron-phonon coupling, but also suggests a new generalized methodology for extracting more quantitative information about electron-phonon coupling constants in quantum materials through comparisons to theory.

Monolayer FeSe films were grown by MBE on undoped $SrTiO_3$ substrates and measured immediately by *in situ* ARPES (He-I photons, $h\nu = 21.2$ eV) as well as *in situ* resistivity measurements (Fig. S1). Having verified their quality and superconducting properties, samples were then capped with ≈100 nm amorphous Se for transport to the Advanced Light Source MAESTRO beamline (7.0.2) in a sealed, inert environment. Films were then decapped at the end station at 420° C, in a vacuum better than 5×10^{-10} Torr immediately prior to ARPES measurements. ARPES measurements were then performed at 15 K at photon energies ranging between 21–75 eV, with a total energy resolution of 10–20 meV (depending on the incident photon energy).

In Fig. 1 we present ARPES measurements of monolayer $FeSe/SrTiO_3$ after decapping, taken at $h\nu = 24$ eV with p-polarized light. Consistent with previous reports, the Fermi surface is comprised of nearly degenerate elliptical electron pockets at M which arise from the glide-mirror symmetry of the iron-selenium plane [15]. Because of the matrix element effects, the electron pocket at M_1 appears with lobes of increased intensity in a threefold pattern about the pocket. In Figs. 1(b) and 1(c), we show raw and second-derivative spectra taken along the $\Gamma - M$ direction as indicated by the blue line in Fig. 1(a). The main band closest to E_F, which we denote as γ, exhibits a well-defined gap and backbending at 15 K, indicative of the expected superconductivity. The first replica band, (γ', red) is visible in the raw ARPES spectra 98 meV below the main band. Two additional, weaker features are also visible in the

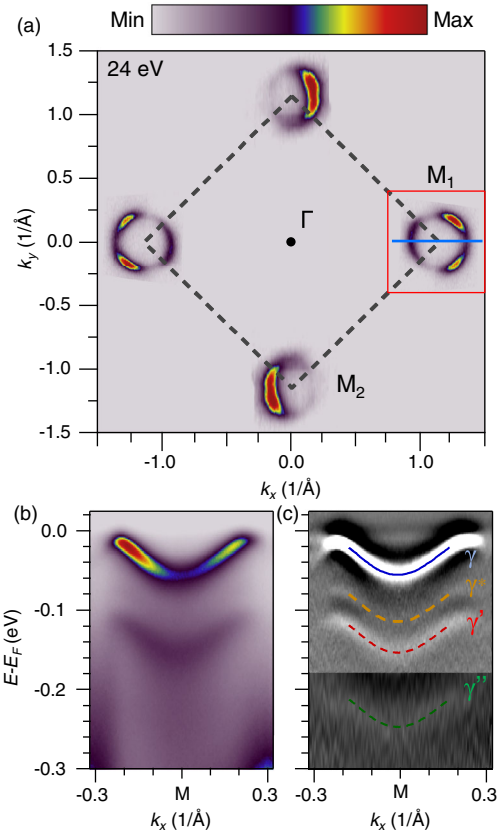

FIG. 1. Fermi surface and replica band topology in single-layer $FeSe/SrTiO_3$. (a) Fermi surface map of single-layer $FeSe/SrTiO_3$ taken with p-polarized light at $h\nu = 24$ eV. (b) High-statistics spectra along the cut shown at M_1 (blue). (c) Second-derivative of the spectra in (b). An additional 60 meV replica (labeled γ^* in the figure) is clearly visible, as well as a second-order replica (labeled γ'') after saturating the color scale over the higher binding energy region.

second-derivative spectra shown in Fig. 1(c), including a faint replica at ≈60 meV (denoted as γ^*, shown in orange), and also an additional replica band separated by 192 meV from the main band (γ'', denoted in green). Their characteristic energies associate them with two distinct Fuchs-Kliewer (FK) phonons of the $SrTiO_3$ substrate, which arise from out-of-plane vibration modes of the oppositely charged Ti and O ions [16]; γ^* corresponds to FK_2, and γ' and γ'' are the first and second-order satellites from FK_1 [17].

If the replica bands indeed arise from extrinsic final-state energy losses, as suggested in Ref. [13], then it is predicted that the ratio of the intensity of the first replica band, γ', relative to the intensity of the main band, γ, $I_{\gamma'}/I_{\gamma}$, should depend strongly on the kinetic energy and direction of the outgoing photoelectron. Conversely, if the replica bands arise from electron-phonon coupling in the initial state, they should be intrinsic features of the single-particle spectral function and hence, the intensity ratio $I_{\gamma'}/I_{\gamma}$ should be insensitive to the photoelectron kinetic energy. In Fig. 2(a),

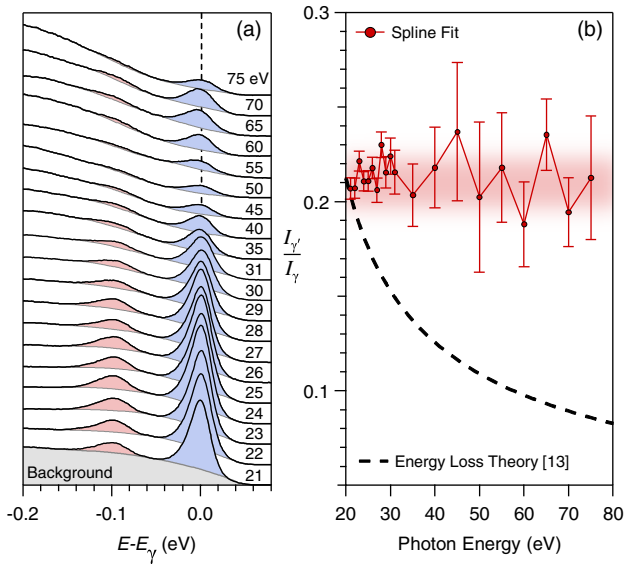

FIG. 2. Photon energy dependence of the replica band intensity. (a) Integrated EDCs collected from $h\nu = 21$ to 75 eV. Grey lines indicate the spline background, while blue and red shaded regions indicate the integrated signal of the γ and γ' bands, respectively. (b) Relative intensity of γ' to γ as a function of incident photon energy (red markers) compared to the theoretical prediction for a photoelectron loss effect from Ref. [13] (black dashed line).

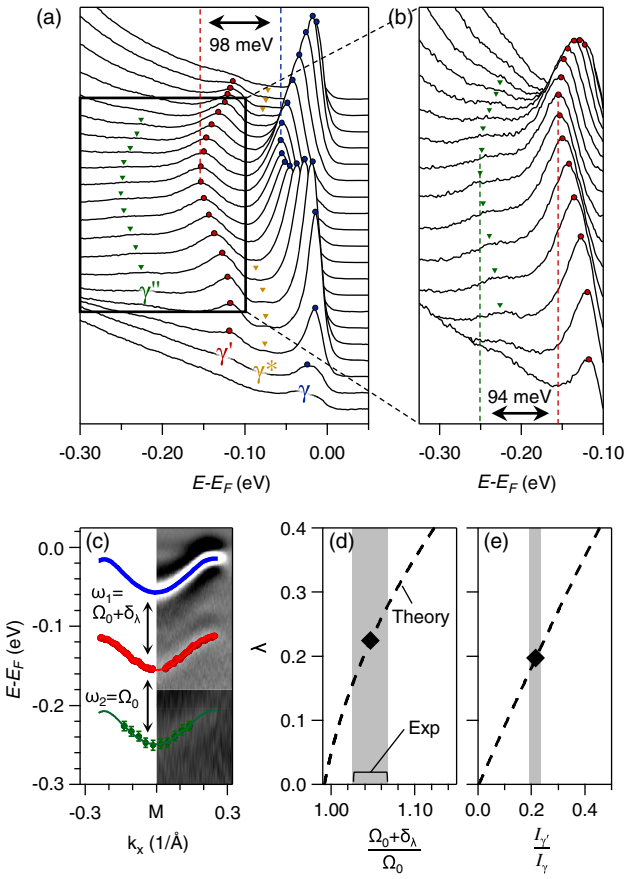

FIG. 3. Observation of second-order replica bands in single-layer FeSe/$SrTiO_3$. (a),(b) EDCs across the spectra at M shown as a waterfall plot. Blue, red, yellow, and green markers track the main band (γ), 98 meV replica (γ'), and 60 meV replica (γ^*), and 190 meV second order replica (γ''), respectively. (c) Band positions based on fits to the EDC peak positions. (d),(e) Determination of the electron-phonon coupling constant λ based on the γ' blueshift (d) and replica band intensity (e). Theoretical behavior based on Ref. [20]. Grey regions indicate the experimental uncertainty.

we plot energy distribution curves (EDCs) around M between 21 eV $< h\nu <$ 75 eV (corresponding to photoelectron kinetic energies between ≈17 to 71 eV). To improve statistics, the EDCs have been generated by integrating over the entire band, offsetting each individual EDC by the peak position of the main band ϵ_k (Fig. S2), then fitted to a smooth spline background with the integrated weight of the main band peak (I_γ) and replica band peak ($I_{\gamma'}$) shown after subtraction in Fig. S3. In Fig. 2(b), we plot the ratio of $I_{\gamma'}/I_\gamma$ as a function of photon energy, which is clearly independent of photon energy, with an extracted value of $I_{\gamma'}/I_\gamma = 0.21 \pm 0.02$, together with a comparison of the prediction for the extrinsic photoelectron energy loss scenario, where a ≈60% reduction in $I_{\gamma'}/I_\gamma$ would have been expected. This is despite the fact that the overall absolute intensity of both I_γ and $I_{\gamma'}$ drops by a factor of 10 in going to higher photon energies (hence the larger error bars for $h\nu > 40$ eV), thus definitively ruling out extrinsic photoelectron loss effects as the origin of the replica band in FeSe/$SrTiO_3$. We have confirmed that this behavior is robust against details of the fitting procedure, for example, whether a single EDC at M is used as opposed to band-averaged spectra, or whether a Shirley background is used in place of a spline fit.

Performing this extensive photon energy dependence study provides the opportunity to extract more detailed information about the electron-phonon coupling than had previously been possible. For one, this analysis allows us to reliably determine the absolute intensity of $I_{\gamma'}/I_\gamma = 0.21 \pm 0.02$. Furthermore, we are now able to identify an optimal photon energy, $h\nu = 24$ eV with p polarization where the intensity of features is strongest, so as to enable a more detailed, quantitative line shape analysis of the spectral function and replica bands. In Figs. 3(a) and 3(b), we show a series of EDCs around M at 24 eV, with the band positions for γ, γ^*, γ', and γ'' indicated by markers. This data allows us to accurately determine the separation between γ and γ' as $\omega_1 = 98 \pm 1$ meV, as well as the separation between the first and second replicas, γ' and γ'', $\omega_2 = 94 \pm 2$ meV, 4 meV less than ω_1. These values for each replica feature, along with estimates of the relative band intensity based on fits to the background-subtracted EDCs (Fig. S6), are shown in Table I. The energy of the FK_1 phonon in the undoped $SrTiO_3$ substrate has previously been determined to be 94 meV [10,18],

TABLE I. Replica band energy offsets and relative intensities for γ^*, γ', and γ'' based on fits to the EDC peak positions [Fig. 3(c)] and line shape (Fig. S6).

Band	Energy offset (meV)	Intensity (I_{γ^n}/I_γ)
γ	0	1.0
γ^*	-59 ± 2	0.02 ± 0.01
γ'	-98 ± 1	0.21 ± 0.02
γ''	-192 ± 2	0.04 ± 0.025

although this value is highly doping dependent [19]. Therefore, the separation between γ and γ' is blueshifted by $\delta_\lambda = 4$ meV, relative to the bare FK_1 phonon energy, as shown in Fig. 3(c). This is in contrast to the separation between γ' and γ'', which closely matches Ω_{KF1} to within experimental error (94 ± 2 meV).

Such a blueshift of the first-order replica (and corresponding lack of a shift for the second-order replica), has been discussed theoretically in various systems [8,20–23], but to our knowledge, this is the first instance where this behavior has been clearly identified experimentally. As has been discussed theoretically, reliably extracting both the blueshift, δ_λ (or alternatively ω_1/ω_2), as well as the intensity ratio between the main and first replica bands, $I_{\gamma'}/I_\gamma$, allows us to more accurately infer the strength of the electron-phonon coupling, which we describe via the dimensionless parameter λ as the Fermi surface average of the momentum-dependent coupling constant $g(\boldsymbol{q}) = g_0 e^{-|q|/q_0}$ used in theoretical models [24–27]. This is of particular importance to the $FeSe/SrTiO_3$ system, since the possible enhancement of T_c due to coupling to interfacial substrate phonons has been shown to vary strongly as a function of λ in certain models [20–22].

Performing accurate and realistic calculations of electron-phonon interactions in quantum materials remains a long-standing theoretical challenge. By simultaneously comparing two independently extracted experimental quantities that are both related to λ, $I_{\gamma'}/I_\gamma$, and ω_1/ω_2, we can tightly constrain existing theoretical calculations of electron-phonon coupling in $FeSe/SrTiO_3$. For previous work based on either single-band or multiband Migdal-Eliashberg calculations [21,22,27], we have found that it is not possible for a single value of λ in the calculations to simultaneously match both our experimentally determined blueshift ($\omega_1/\omega_2 = 1.045 \pm 0.025$) as well as intensity ratio ($I_{\gamma'}/I_\gamma = 0.21 \pm 0.02$). For instance, in Ref. [22], a theoretical value of $\lambda \approx 0.2$ is needed to match the experimental blueshift, ω_1/ω_2, whereas a value of $\lambda \approx 1.05$ is needed to match the experimental intensity ratio, as shown in Fig. S4 (we note that $\lambda \approx 4.17\lambda_m$ for forward scattering of $q_0 = 0.1/a$ [22,26]). Alternatively, we find that prior calculations by Li *et al.* based on sign-problem-free quantum Monte Carlo simulations of $FeSe/SrTiO_3$ in the presence of strong forward scattering yield values of $I_{\gamma'}/I_\gamma$ and ω_1/ω_2 that agree with our experiments for a single value of $\lambda = 0.19 \pm 0.02$ [20]. The theoretical results in this limit of small momentum transfer for both $I_{\gamma'}/I_\gamma$ and δ_λ are reproduced as dashed lines in Figs. 3(d) and 3(e), together with our experimentally determined values for both quantities (shown as shaded bars, which denote our experimental uncertainty).

For a value of $\lambda = 0.19$, calculations by Li *et al.* would suggest an interfacial enhancement of Δ of $\approx 11\%$ [20]. While considerable, this cannot entirely account for a gap closing temperature of 60–70 K compared to bulk electron-doped FeSe compounds ($T_c \approx 40$ K), indicating that other effects might be at play. Combined *in situ* resistivity and ARPES measurements have revealed the presence of a pseudogap above 40 K in monolayer $FeSe/SrTiO_3$ [28]. A similar pseudogap phase has also been reported in the highly two-dimensional bulk intercalated compound $(TBA^+)FeSe$ up to 60 K ($c = 15.5$ Å; $\rho_c/\rho_{ab} \approx 10^5$) [29], which is absent any interfacial effects, suggesting that enhanced pre-formed pairing in monolayer $FeSe/SrTiO_3$ and $(TBA^+)FeSe$ could arise predominantly from the enhanced two dimensionality of the electronic structure. This could also explain why the reported gap closing temperatures in monolayer $FeSe/SrTiO_3$ are universally high, even when the replica bands are fairly weak or not observed [30–34]. Nevertheless, given that the observed replica bands arise from intrinsic interfacial electron-phonon coupling, our result suggests that engineering alternative interface systems with stronger λ may offer a means by which to achieve a more substantial enhancement in monolayer superconducting films.

In addition to the blueshift and intensity ratios, a detailed analysis of the spectral function also reveals evidence for electron-phonon coupling in the lifetime broadening of the first replica band, $\Gamma_{\gamma'}$ relative to that of the main band, Γ_γ (the second replica, γ'', is too weak to allow a reliable analysis of its line shape). In Fig. 4(a), we show the extracted spectral function after fitting to the backgrounds used in Fig. 2 (as before, our conclusions here are independent of the specific background that is employed, Fig. S5). The expected sharpening of the main band peak, Γ_γ, as it approaches E_F can be clearly observed in Fig. 4(b), where we plot Γ as a function of binding energy E_B. Likewise, the scattering rate of the first replica band, $\Gamma_{\gamma'}$, exhibits similar behavior, but with the minimum value of $\Gamma_{\gamma'}$ (at k_F) approximately equal to the maximum value of Γ_γ (taken at the band bottom, M), as would be expected if both features naturally arise from a single, intrinsic spectral function. For comparison, we also plot the simulated linewidth of the first replica, $\Gamma_{\gamma'}$ in the extrinsic photoelectron loss scenario, where the width would correspond to that of the main band γ convoluted with the lifetime of the FK_1 phonon, Γ_{FK1} [19]. As can be seen in Fig. 4(b), the experimentally determined value of $\Gamma_{\gamma'}$ is substantially larger than would be expected in a

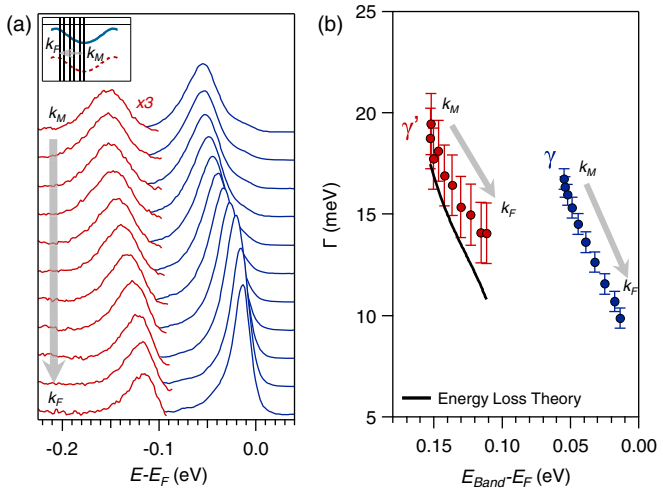

FIG. 4. Quasiparticle lifetime broadening in the replica band. (a) Background-subtracted EDCs spanning the electron pocket dispersion, from the band bottom (k_M) to k_F, for data taken at $h\nu = 24$ eV. The γ' feature has been multiplied by 3 for visual clarity. (b) Quasiparticle lifetimes based on spectral function fits for γ (blue) and γ' (red). The solid black line indicates the anticipated replica band behavior under the extrinsic photoelectron energy loss scenario.

photoelectron loss scenario, once again pointing towards its intrinsic character.

In summary, we have performed an extensive quantitative analysis of replica bands in the ARPES line shape of single-layer $FeSe/SrTiO_3$, which allows us to reliably extract both the blueshift of the first replica band, δ_λ, and the intensity ratio $I_{\gamma'}/I_\gamma$ between the replica and main bands. A comparison with theoretical calculations in the limit of strong forward scattering allows us to accurately determine the strength of the coupling between electrons in the FeSe layer and Fuchs-Kliewer phonons in the $SrTiO_3$ substrate as $\lambda = 0.19 \pm 0.02$, suggesting that the enhancement of the superconducting gap from interfacial coupling is approximately 11%. This implies that interfacial coupling alone may not account for the enhanced gap closing temperature reported by ARPES. Our reliable quantification of the replica band parameters provides important constraints for theoretical studies of the forward-scattering electron-phonon interaction in the $FeSe/SrTiO_3$ system. More generally, our analysis suggests a new methodology for comparisons with theory and quantitatively extracting electron-phonon coupling constants.

This work was primarily supported through the Air Force Office of Scientific Research through Grants No. FA9550-21-1-0168 and No. FA9550-15-1-0474. This work was also supported through the National Science Foundation through NSF DMR-1709255 and the Platform for the Accelerated Realization, Analysis, and Discovery of Interface Materials (PARADIM) under Cooperative Agreement No. DMR-1539918. This research is funded in part by the Gordon and Betty Moore Foundation's EPiQS Initiative through Grant No. GBMF3850 to Cornell University. B. D. F. and J. N. N. acknowledge support from the NSF Graduate Research Fellowship under Grant No. DGE-1650441. P. M. acknowledges support from the Indo US Science and Technology Forum (IUSSTF). This work made use of the Cornell Center for Materials Research (CCMR) Shared Facilities, which are supported through the NSF MRSEC Program (No. DMR-1719875). This research used resources of the Advanced Light Source, a U.S. DOE Office of Science User Facility under Contract No. DE-AC02-05CH11231. Substrate preparation was performed in part at the Cornell NanoScale Facility, a member of the National Nanotechnology Coordinated Infrastructure (NNCI), which is supported by the NSF (Grant No. ECCS-1542081).

*Corresponding author.
bdf53@cornell.edu
†Corresponding author.
kmshen@cornell.edu
‡Present address: Pritzker School of Molecular Engineering, The University of Chicago, Chicago, Illinois 60637, USA.
§Present address: Department of Materials Science and Engineering, University of Wisconsin, Madison, Wisconsin 53706, USA.
‖Present address: Department of Physics, Indian Institute of Science, Bangalore 560012, India.

[1] A. Lanzara, P. V. Bogdanov, X. J. Zhou, S. A. Kellar, D. L. Feng, E. D. Lu, T. Yoshida, H. Eisaki, A. Fujimori, K. Kishio, J.-I. Shimoyama, T. Noda, S. Uchida, Z. Hussain, and Z.-X. Shen, Nature (London) **412**, 510 (2001).
[2] X. J. Zhou *et al.*, Nature (London) **423**, 398 (2003).
[3] N. Mannella, W. L. Yang, X. J. Zhou, H. Zheng, J. F. Mitchell, J. Zaanen, T. P. Devereaux, N. Nagaosa, Z. Hussain, and Z.-X. Shen, Nature (London) **438**, 474 (2005).
[4] Z. Wang *et al.*, Nat. Mater. **15**, 835 (2016).
[5] C. Chen, J. Avila, E. Frantzeskakis, A. Levy, and M. C. Asensio, Nat. Commun. **6**, 8585 (2015).
[6] C. Zhang, Z. Liu, Z. Chen, Y. Xie, R. He, S. Tang, J. He, W. Li, T. Jia, S. N. Rebec, E. Y. Ma, H. Yan, M. Hashimoto, D. Lu, S.-K. Mo, Y. Hikita, R. G. Moore, H. Y. Hwang, D. Lee, and Z. Shen, Nat. Commun. **8**, 14468 (2017).
[7] S. Moser, L. Moreschini, J. Jaćimović, O. S. Barišić, H. Berger, A. Magrez, Y. J. Chang, K. S. Kim, A. Bostwick, E. Rotenberg, L. Forró, and M. Grioni, Phys. Rev. Lett. **110**, 196403 (2013).
[8] C. Verdi, F. Caruso, and F. Giustino, Nat. Commun. **8**, 15769 (2017).
[9] J. J. Lee, F. T. Schmitt, R. G. Moore, S. Johnston, Y.-T. Cui, W. Li, M. Yi, Z. K. Liu, M. Hashimoto, Y. Zhang, D. H. Lu, T. P. Devereaux, D.-H. Lee, and Z.-X. Shen, Nature (London) **515**, 245 (2014).
[10] Q. Song, T. L. Yu, X. Lou, B. P. Xie, H. C. Xu, C. H. P. Wen, Q. Yao, S. Y. Zhang, X. T. Zhu, J. D. Guo, R. Peng, and D. L. Feng, Nat. Commun. **10**, 758 (2019).

[11] X. Shi, Z.-Q. Han, X.-L. Peng, P. Richard, T. Qian, X.-X. Wu, M.-W. Qiu, S. C. Wang, J. P. Hu, Y.-J. Sun, and H. Ding, Nat. Commun. **8**, 14988 (2017).
[12] M. Yang, C. Yan, Y. Ma, L. Li, and C. Cen, Nat. Commun. **10**, 85 (2019).
[13] F. Li and G. A. Sawatzky, Phys. Rev. Lett. **120**, 237001 (2018).
[14] R. Fuchs and K. L. Kliewer, Phys. Rev. **140**, A2076 (1965).
[15] Y. Zhang, J. J. Lee, R. G. Moore, W. Li, M. Yi, M. Hashimoto, D. H. Lu, T. P. Devereaux, D.-H. Lee, and Z.-X. Shen, Phys. Rev. Lett. **117**, 117001 (2016).
[16] H. Vogt, Phys. Rev. B **38**, 5699 (1988).
[17] S. Zhang, J. Guan, X. Jia, B. Liu, W. Wang, F. Li, L. Wang, X. Ma, Q. Xue, J. Zhang, E. W. Plummer, X. Zhu, and J. Guo, Phys. Rev. B **94**, 081116(R) (2016).
[18] T. Conard, L. Philippe, P. Thiry, P. Lambin, and R. Caudano, Surf. Sci. **287–288**, 382 (1993).
[19] S. Zhang, J. Guan, Y. Wang, T. Berlijn, S. Johnston, X. Jia, B. Liu, Q. Zhu, Q. An, S. Xue, Y. Cao, F. Yang, W. Wang, J. Zhang, E. W. Plummer, X. Zhu, and J. Guo, Phys. Rev. B **97**, 035408 (2018).
[20] Z.-X. Li, T. P. Devereaux, and D.-H. Lee, Phys. Rev. B **100**, 241101(R) (2019).
[21] F. Schrodi, A. Aperis, and P. M. Oppeneer, Phys. Rev. B **98**, 094509 (2018).
[22] L. Rademaker, Y. Wang, T. Berlijn, and S. Johnston, New J. Phys. **18**, 022001 (2016).
[23] M. L. Kulić and O. V. Dolgov, New J. Phys. **19**, 013020 (2017).
[24] Z.-X. Li, F. Wang, H. Yao, and D.-H. Lee, Sci. Bull. **61**, 925 (2016).
[25] Y. Wang, A. Linscheid, T. Berlijn, and S. Johnston, Phys. Rev. B **93**, 134513 (2016).
[26] Y. Wang, K. Nakatsukasa, L. Rademaker, T. Berlijn, and S. Johnston, Supercond. Sci. Technol. **29**, 054009 (2016).
[27] A. Aperis and P. M. Oppeneer, Phys. Rev. B **97**, 060501(R) (2018).
[28] B. D. Faeth, S. Yang, J. K. Kawasaki, J. N. Nelson, P. Mishra, C. T. Parzyck, C. Li, D. G. Schlom, and K. M. Shen, Phys. Rev. X **11**, 021054 (2021).
[29] B. L. Kang, M. Z. Shi, S. J. Li, H. H. Wang, Q. Zhang, D. Zhao, J. Li, D. W. Song, L. X. Zheng, L. P. Nie, T. Wu, and X. H. Chen, Phys. Rev. Lett. **125**, 097003 (2020).
[30] D. Liu, W. Zhang, D. Mou, J. He, Y. Ou, Q.-Y. Wang, Z. Li, L. Wang, L. Zhao, S. He, Y. Peng, X. Liu, C. Chen, L. Yu, G. Liu, X. Dong, J. Zhang, C. Chen, Z. Xu, and X. J. Zhou, Nat. Commun. **3**, 931 (2012).
[31] S. Tan, Y. Zhang, M. Xia, Z. Ye, F. Chen, X. Xie, R. Peng, D. Xu, Q. Fan, H. Xu, J. Jiang, T. Zhang, X. Lai, T. Xiang, J. Hu, B. Xie, and D. Feng, Nat. Mater. **12**, 634 (2013).
[32] J. He, X. Liu, W. Zhang, L. Zhao, D. Liu, S. He, D. Mou, F. Li, C. Tang, Z. Li, L. Wang, Y. Peng, Y. Liu, C. Chen, L. Yu, G. Liu, X. Dong, J. Zhang, C. Chen, Z. Xu, X. Chen, X. Ma, Q. Xue, and X. J. Zhou, Proc. Natl. Acad. Sci. U.S.A. **111**, 18501 (2014).
[33] R. Peng, X. P. Shen, X. Xie, H. C. Xu, S. Y. Tan, M. Xia, T. Zhang, H. Y. Cao, X. G. Gong, J. P. Hu, B. P. Xie, and D. L. Feng, Phys. Rev. Lett. **112**, 107001 (2014).
[34] R. Peng, H. C. Xu, S. Y. Tan, H. Y. Cao, M. Xia, X. P. Shen, Z. C. Huang, C. H. P. Wen, Q. Song, T. Zhang, B. P. Xie, X. G. Gong, and D. L. Feng, Nat. Commun. **5**, 5044 (2014).
[35] See Supplemental Material at http://link.aps.org/supplemental/10.1103/PhysRevLett.127.016803 for details on *in situ* characterization of single-layer $FeSe/SrTiO_3$ films, information regarding the ARPES data processing, background subtraction, and fitting procedures, and a comparison of results when extracting λ using different theoretical predictions [20,22].

Interfacial Electron-Phonon Coupling Constants Extracted from Intrinsic Replica Bands in Monolayer FeSe/$SrTiO_3$ - SUPPLEMENTAL MATERIAL

Brendan D. Faeth,[1] Saien Xie,[1] Shuolong Yang,[1,2,3] Jason K. Kawasaki,[1,2] Jocienne N. Nelson,[1] Shuyuan Zhang,[1] Christopher Parzyck,[1] Pramita Mishra,[1] Chen Li,[1] Christopher Jozwiak,[4] Aaron Bostwick,[4] Eli Rotenberg,[4] Darrell G. Schlom,[3,2] and Kyle M. Shen[1,2]

[1]*Department of Physics, Laboratory of Atomic and Solid State Physics, Cornell University, Ithaca, New York 14853, USA*
[2]*Kavli Institute at Cornell for Nanoscale Science, Ithaca, NY 14853, USA*
[3]*Department of Materials Science and Engineering, Cornell University, Ithaca, NY 14853, USA*
[4]*Advanced Light Source, E.O. Lawrence Berkeley National Laboratory, Berkeley, CA 94720, USA*

---

[1] Z.-X. Li, T. P. Devereaux, and D.-H. Lee, Phys. Rev. B **100**, 241101 (2019).

[2] L. Rademaker, Y. Wang, T. Berlijn, and S. Johnston, New Journal of Physics **18**, 022001 (2016).

[3] P. Steiner, H. Höchst, and S. Hüfner, "Simple metals," in *Photoemission in Solids II: Case Studies*, edited by L. Ley and M. Cardona (Springer Berlin Heidelberg, Berlin, Heidelberg, 1979) pp. 349–372.

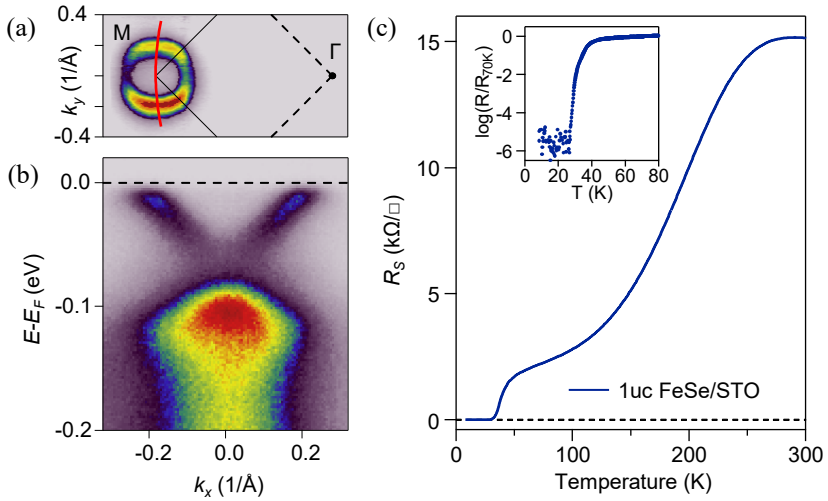

Figure S1. **Combined *in situ* ARPES and electrical resistivity measurement of monolayer FeSe/SrTiO$_3$ prior to transportation to ALS.** (**a**) Fermi surface intensity map for an as-grown monolayer FeSe/SrTiO$_3$ sample held at 12 K, integrated over ± 5 meV of E_F. The black solid line indicates the boundary of the 2-Fe Brillouin zone. (**b**) Photoemission intensity at M (red line in Panel A) taken at 12 K. ARPES measurements shown in (a) and (b) were performed using a He plasma lamp with unpolarized light, $h\nu = 21.2$ eV. (**c**) Temperature-dependent sheet resistance for the identical film measured *in situ* in a vacuum better than 1×10^{-10} Torr. The inset shows the low temperature data in log scale.

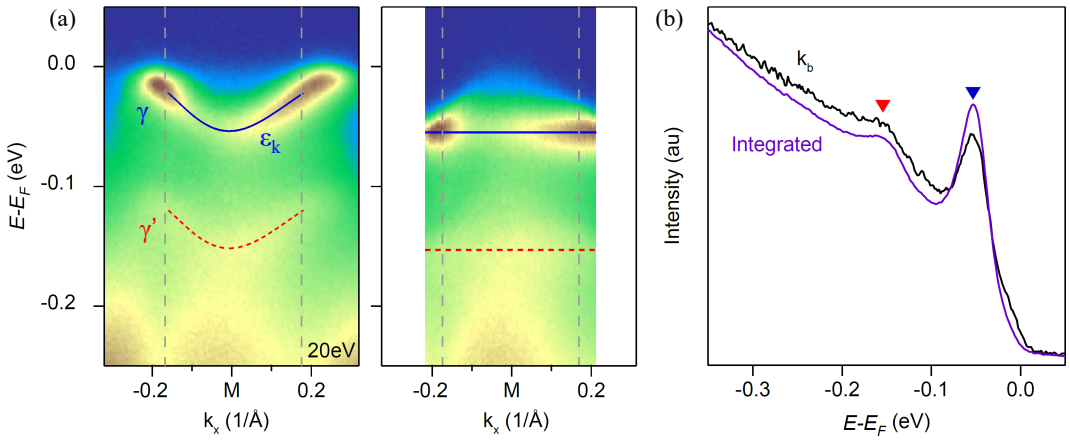

Figure S2. **Processing procedure used to generate integrated EDC's around the electron pocket at M.** (**a**) Example 20 eV ARPES spectra at M before (left) and after (right). Blue and red dashed lines highlight the EDC peak positions for the main and replica bands, respectively. (**b**) EDC's are then integrated over the inner 80% of k_F (within the dashed grey lines in (a)) to produce the purple curve, shown in comparison to a raw EDC collected at M (black). Data presented in Fig. 2(a) of the main text are integrated over both k_x and k_y within the equivalent region around M.

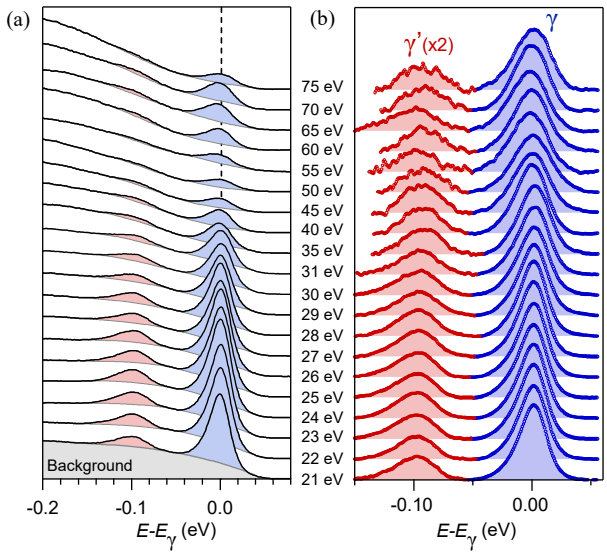

Figure S3. **Photon energy dependent EDC's after background subtraction.** (**a**) Integrated EDC's collected from $h\nu$ = 21 to 75 eV, as shown in Fig. 2(a). (**b**) The same data as in (a), after subtracting the spline background from each EDC. The γ' feature is multiplied by 2 for visual clarity.

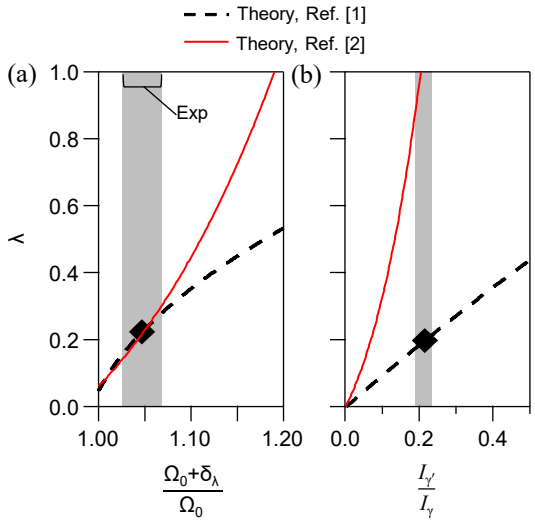

Figure S4. **Extraction of λ based on comparison to theory.** Determination of the electron-phonon coupling constant λ based on the blue shift (a) and replica band intensity (b). Grey regions indicate the experimental uncertainty. Dashed black line is theoretical behavior predicted by Ref. [1], and the red solid line is the equivalent predicted behavior from Ref. [2].

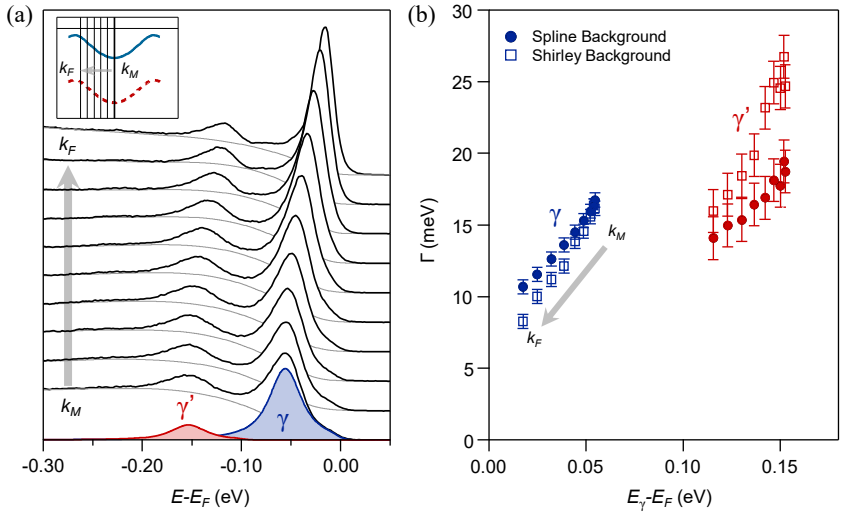

Figure S5. **Influence of background function on quasiparticle lifetime analysis.** (**a**) EDC's spanning the electron pocket dispersion, from the band bottom (k_M) to k_F. Light grey lines indicate a spline fit to the background, and blue and red regions show example fits to the quasiparticle peaks at k_M after background subtraction. (**b**) Comparison of extracted peak half-widths Γ when using either a spline (solid symbols) or Shirley (open symbols) background function.

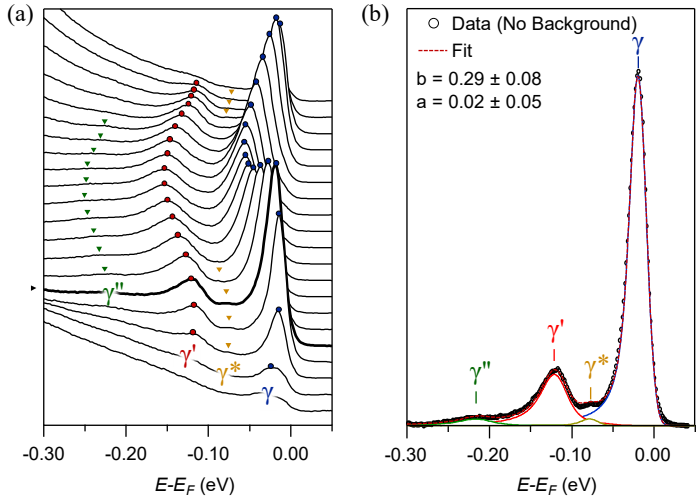

Figure S6. **Fitting of the second-order replica band intensity.** A further consistency check of the probabilities of intrinsic and extrinsic energy losses can be performed by comparing the relative intensities of γ, γ', and γ''. (a) EDCs across M, duplicated from Fig. 3(a) of the main text. k_F is highlighted with a thicker line and arrow marker. (b) Fitting of the spline background-subtracted EDC near k_F (where the weaker γ'' replica band is most visible, black markers) to a four peak model with the intensities of γ' and γ'' restricted to Eq. 7.16 from Steiner, Hochst, and Hufner [3], such that $I_{\gamma^n} = I_0 \left(\frac{e^{-b} b^{-n}}{n!} + a \frac{I_{n-1}}{I_0} \right)$. Blue, orange, red, and green peaks indicate the fitted peak shapes for γ, γ^*, γ', and γ'', respectively. Despite the low overall intensity of the second-order replica, we obtain a reasonable fit with parameters b (corresponding to intrinsic coupling) = 0.29 ± 0.08 and a (corresponding to extrinsic losses) = 0.02 ± 0.05, consistent with the expectation for almost exclusively intrinsic replica features.